NJC

ROYAL SOCIETY OF CHEMISTRY

PAPER

View Article Online
View Journal | View Issue

Cite this: *New J. Chem.*, 2021, **45**, 4694

Preparation and photocatalytic performance of silver-modified and nitrogen-doped TiO_2 nanomaterials with oxygen vacancies

Hong Zhang, [a] Yingyu Jiang, [ab] Baiqin Zhou, [c] Zhuo Wei, [a] Zhenya Zhu, [a] Lijuan Han, *[b] Ping Zhang *[a] and Yingying Hu [b]

Received 26th September 2020,
Accepted 25th January 2021

DOI: 10.1039/d0nj04755d

rsc.li/njc

The photocatalysis of titanium dioxide (TiO_2) exerts excellent degradation performance against contaminants in the environment. However, it prefers to absorb ultraviolet light rather than visible light, which significantly constrains its widespread use under visible light. Here, we prepared oxygen vacancy-containing TiO_2 *via* Ag-modification and N-doping. The utilization of visible light for phenol degradation was significantly enhanced by Ag/N co-doping. The characterization results showed a shuttle-like material coupled with multiple oxygen vacancies, and a well-designed experiment demonstrated that the Ti : N : Ag ratio of 1 : 0.45 : 0.32 presented optimal performance for phenol degradation. The batch experiment results also proved the modified TiO_2 as a potent photocatalyst against phenol degradation with an 80.8% degradation efficiency within 5 hours under visible light and with a 99.3% degradation efficiency within 2 hours under ultraviolet light. What is more, we also demonstrated that hydroxyl radical was the mainly effective radical in the mineralization of phenol and put forward a possible degradation pathway based on the observed intermediates. Lastly, the cycling tests indicated that the proposed photocatalyst is durable with a fair phenol degradation ability after recycling 5 times.

1. Introduction

Since the phenomenon of water decomposition by titanium dioxide (TiO_2) photocatalysts was first observed in 1970s, the use of TiO_2 in environmental applications has stimulated a lot of interest among scholars.[1,2] Due to its high catalytic efficiency, stable chemical properties and non-toxicity, studies on the use of TiO_2 in wastewater treatment have continued for nearly 5 decades.[3,4] Under light source stimulation, TiO_2 generates extremely active free radicals,[5,6] which could despoil the electrons of organic matters and induce an ensuing chain reaction, thus efficiently degrading pollutants and purifying water.[7–10]

However, some drawbacks of TiO_2 also constrain its wide application. The band gap of pure TiO_2 is wide ranging from 3.16 to 3.2 eV, which means that more light energy input is needed to stimulate electron jumping from the valence band to the conduction band. Compounding the problem, the band edge of pure TiO_2 is located in the ultraviolet light region, and therefore pure TiO_2 prefers to absorb ultraviolet light---accounting for only about 4% of the entire solar spectrum—rather than visible light, significantly restricting its wider application in a realistic environment.[11–13] A feasible method to solve this problem is to dope precious metal particles (such as Au, Pt, and Ag) onto the surface of TiO_2, which extends the spectral response to the visible region. Bouhadoun *et al.*[14] synthesized TiO_2 and Au modified TiO_2 (Au–TiO_2) nanoparticles. The photocatalytic activities of the two powders were evaluated by the photocatalytic degradation of formic acid (FA) under ultraviolet and visible light irradiation. Under ultraviolet light irradiation, both samples showed a higher catalytic efficiency compared with the commercial TiO_2 P25. In addition, Au modification, even at very low concentrations, increased the photocatalytic activity to a great degree, and this performance was starker under visible light. Ge *et al.*[15] used an *in situ* deposition technology to uniformly disperse Ag particles inside and outside of vertically aligned TiO_2 nanotubes. The results showed that the deposition of Ag nanoparticles (AgNPs) significantly enhanced the response of TiO_2 nanotubes to visible light. It was found that, in the AgNPs/TiO_2 semiconductor system, AgNPs played a key role in visible light absorption due to the localized surface plasmon resonance (LSPR) effect.[16] Wang *et al.*[17] also observed similar findings, demonstrating that Ag modification is a powerful factor in photocatalysis with maximum H_2 evolution, as a result of strong LSPR. Simultaneously, the surface-formed

[a] *School of Chemical Engineering, Northwest Minzu University, Lanzhou, 730070, Gansu, China. E-mail: zhangping@xbmu.edu.cn*
[b] *Gansu Natural Energy Insititue, Gansu Academy of Sciences, Lanzhou, 730070, Gansu, China. E-mail: ljhanzhang@163.com*
[c] *School of Civil and Environmental Engineering, Harbin Institute of Technology (Shenzhen), Shenzhen, 518055, China*

Schottky barrier of the material, which resulted from LSPR, strongly hindered photo-generated electron–hole recombination, thus improving its photocatalytic ability. Furthermore, other opinions were that metal-donated electrons efficiently filled photo-generated holes, and then unrecombined photo-generated electrons can bombard the absorbed oxygen to form superoxide radical anion ($^{\bullet}O_2^-$) on the surface, leading to a better photocatalytic performance.[18] Besides metal-doping, other methods, such as non-metal doping, defect control, semiconductor compounding, and dye sensitization, were also demonstrated to be useful.[19,20] Among these methods, nitrogen-doping has been regarded as the most promising one for improving catalytic performance.[21] Numerous studies[22] found that the substitution of O by element N in the TiO_2 crystal lattice narrowed the band gap of TiO_2 to some degree, enhancing its response to visible light.[23] Senthilnathan *et al.*[24] found that N-doped titanium dioxide (N-TiO_2) degraded the insecticide lindane under visible light with a striking efficiency of ~100%. Ibukun *et al.*[25] prepared N-TiO_2 by a hydrothermal method and modified it by air plasma treatment. Compared with the band gap of pure TiO_2 of 3.1 eV, the band gap of N-TiO_2 reduced to 2.7 eV, and the photocurrent response by N-TiO_2 increased 3.6 times. Lee H. U. *et al.*[26] used an improved sol–gel method coupled with ultrasonic irradiation to synthesize nano-porous N-TiO_2 at room temperature without heat treatment, also making it more efficient to use visible light.

Herein, we balanced the merits of metal Ag and non-metal N, and synthesized Ag-modified, N-doped and shuttle-like TiO_2. We first reported an improved hydrothermal method for this material synthesis. In the synthesis method of our experiment, $NH_3{\cdot}H_2O$ was used as the nitrogen source and also acted as a settling agent and a solvent. This tactic greatly simplified the operation and was more practical compared with other methods.[27] Furthermore, once $AgNO_3$ was added into $NH_3{\cdot}H_2O$, silver ammonia solution formed, which benefited *in situ* reactions between Ag and Ti elements. Many other factors, for instance, temperature, addition amount, and different additive ratios, were also considered in the synthesis to simplify the whole process referred from Eryk Fernandes *et al.*[27] Meanwhile, phenol was selected as the target for catalytic performance testing, and multiple characterizations were also applied to elucidate the mechanisms including the effects of three free radicals ($^{\bullet}O_2^-$, $^{\bullet}OH$ and h^+). The purpose of this study was to design a rational, potent and economic semiconductor, and to offer some clues in exploring the mechanisms of photocatalysis.

2. Materials and methods

2.1. Instruments and chemicals

The crystal structures of the samples were obtained using an X-ray diffraction (XRD, PANalytical, The Netherlands) instrument with Cu-Kα as the radiation source. The chemical states of elements in the materials were measured using an X-ray photoelectron spectroscopy (XPS, ESCALAB, USA) analyzer. The morphology and structure of the sample were detected using a field emission scanning electron microscope (SEM, JEOL, Japan), a transmission electron microscope (TEM, FEI, USA) and a high resolution transmission electron microscope (HRTEM, JEOL, Japan). The organic carbon content in wastewater was measured through a total organic carbon (TOC, Shimadzu, Japan) analyzer. The concentration of the solution was measured using a high performance liquid chromatograph (HPLC, Shimadzu, Japan). An ultrasonic oscillator (KQ-500E, Keqiao, Dongguan) was used to achieve uniform dispersion of the materials. A high-speed centrifuge rotator (TGL-20B, Anting, Shanghai) was used for centrifugal separation. A constant temperature blast drying oven (HS-9000A, Hesheng, Shanghai) was employed to dry the materials. A photo-chemical reaction instrument (PCX50A, Pofilai, Beijing) was applied for the photocatalytic reaction.

Ammonia solution ($NH_3{\cdot}H_2O$, AR, ≥25%) and titanium butoxide ($C_{16}H_{36}O_4Ti$, AR, ≥99%) were purchased from Tianjin Guangfu Fine Chemical Research Institute; sodium hydroxide (NaOH, AR, ≥96%) was obtained from Shanghai Wokai Biotechnology Co., Ltd; silver nitrate ($AgNO_3$, AR, ≥99.8%) was purchased from Shanghai Zhongqin Chemical Reagent Co., Ltd; phenol (C_6H_6O, AR, ≥99.5%) was purchased from Tianjin Fuchen Chemical Reagent Factory; deionized water (H_2O) was purchased from Wahaha Beverage Co., Ltd, and ethanol (C_2H_5OH, AR, ≥99.9%) was purchased from Sinopharm Group Chemical Reagent Co., Ltd.

2.2. Experimental method

In a typical synthesis process, 7.8 ml tetra-*n*-butyl titanate and 68 ml $NH_3{\cdot}H_2O$ solution were added into a flask to form a mixture under magnetic stirring for 2 h. After that, the mixture was further processed hydrothermally in a polytetrafluoroethylene reactor for 24 h. After it was cooled down to room temperature, the precursor was washed with deionized water until a constant supernatant pH was achieved. In order to investigate the effect of synthesis temperature on the performance of N-doped TiO_2, three heating temperatures were selected, namely, 150 °C, 180 °C, and 210 °C. The obtained samples were labelled as T_1-N-TiO_2, T_2-N-TiO_2 and T_3-N-TiO_2, respectively. Furthermore, we also selected several quantum 12 h, 24 h, 36 h, 48 h and 60 h to investigate the effect of residence time on catalyst structure and catalytic performance. Additionally, the influence of Ag-doping was also investigated; $AgNO_3$ solutions with different concentrations were separately added drop-wise into the flask after the solution of tetra-*n*-butyl titanate and $NH_3{\cdot}H_2O$ was stirred and mixed for 2 h. The follow-up hydrothermal process was the same as mentioned above.

2.3. Removal of phenol under different light sources

The light source used was a Multi-channel Photo-chemical Reaction Instrument (PCX50A, Beijing Bofeilai Technology Co., Ltd) with a 420 nm LED light source as the visible light source and a 365 nm LED light source as the ultraviolet light source. The incident intensities of ultraviolet light and visible light were 7.4 μW cm^{-2} and 8.3 μW cm^{-2}, respectively. Phenol was chosen as the contaminant for the degradation study. The volume of the phenol solution was 50 mL with an initial concentration of 10 mg L^{-1}, and the addition amount of catalyst was 50 mg. After the adsorption equilibrium of phenol

in a dark environment was obtained, the photocatalysis was started by applying a light source for phenol degradation. Samples were collected at 0 h, 0.5 h, 1 h, 1.5 h, 2 h, 3 h, 4 and 5 h. The remaining phenol concentration in the solution was measured using a HPLC analyzer and a TOC analyzer. The removal amount, removal rate, and mineralization rate were expressed using the following formula:

$$R = [(C_{\rho 0} - C_{\rho t})/C_{\rho 0}] \times 100\% \quad (1)$$

$$Q = [(C_0 - C_t)/C_0] \times 100\% \quad (2)$$

where R is the phenol removal rate at the objective time (%); $C_{\rho 0}$ and $C_{\rho t}$ are the concentrations of phenol at the initial and objective times, respectively (mg L^{-1}); Q is the mineralization of phenol at the objective time (%); and C_0 and C_t represent the organic carbon contents of phenol at initial and objective times, respectively (mg L^{-1}).

3. Results and discussion

3.1. Structures and morphology of photocatalysts

3.1.1. X-ray diffraction (XRD) analysis. Fig. 1(a) shows the XRD patterns of N-TiO_2 prepared at different hydrothermal reaction temperatures. The standard comparison cards of anatase and rutile TiO_2 are also shown in the same figure for comparison. Fig. 1(b) presents the XRD patterns of Ag/N-TiO_2 prepared at different reaction times, coupled with the standard comparison cards of anatase TiO_2 and elemental Ag. The strong diffraction peaks at 2θ = 25.3°, 37.8°, 48.0°, 53.9°, 55.1°, and 62.7° corresponding to the (101), (004), (200), (105), (211) and (204) crystal planes of anatase TiO_2, respectively, indicated that anatase TiO_2 was the dominant TiO_2 component produced in our synthesis method. Additionally, the crystal phase of N-TiO_2 (nTi : nN = 1 : 0.45) displayed the optimal crystal at a hydrothermal temperature of 210 °C (shown in Fig. 1(a)). After Ag modification, the (101) peak shifted slightly from 25.3° to 25.7°, implying that surface deposition occurred through Ag modification.[28] Also noticeably, both N-doping and Ag-deposition did not change the general crystallite of TiO_2, revealing an unessential role of O vacancy influencing the TiO_2 crystallite.[23–26] For the effective photocatalytic activity of TiO_2, the crystalline phase is very important. For example, anatase TiO_2 is more active than rutile and brookite TiO_2 in photocatalysis, meaning that a more efficient catalyst was synthesized in this study.[29] Furthermore, in Fig. 1(b), several diffraction peaks located at 2θ = 38.3°, 43.9°, 65.0°, and 77.0° appeared, which originated from the (111), (200), (220), (211) and (311) crystal planes of Ag particles, demonstrating the successful synthesis of the Ag and N co-doped TiO_2 photocatalyst.

3.1.2. X-ray photoelectron spectroscopy (XPS) analysis. The XPS results are shown in Fig. 2. It can be seen that Ag/N-TiO_2 mainly contained five elements, namely, C, Ag, N, Ti and O. Fig. 2(b) shows the Ti 2p spectrum of Ag/N-TiO_2. The peaks at 458.5 eV and 464.3 eV corresponded to Ti $2p_{3/2}$ and Ti $2p_{1/2}$, respectively, which belong to the characteristic 2p peak of Ti^{4+} in TiO_2.[30] No Ti–N or Ti–C bond was observed in the Ti 2p spectrum, indicating that the C and N elements did not enter the TiO_2 lattice during the synthesis.[31] Fig. 2(c) shows several decomposed peaks of O 1s, where the peak at 531.5 eV corresponded to the Ag–O bond and the peak at 529.7 eV corresponded to the Ti–O bond. The peak at 533.2 eV corresponded to the O vacancy bond, and the generally large area of this peak also suggested the existence of a large number of O vacancies, which mainly originated from the TiO_2 lattice. Fig. 2(d) shows the N 1s absorption peak, and the peak at a low binding energy of 399.5 eV originated from sp hybridization. In TiO_2, N formed interstitial nitrogen to form Ti–N–O or Ti–O–N bonds. The nitrogen–oxygen bond, that is, the N element was doped into the TiO_2 lattice by gap doping, and oxygen defects formed. The result was consistent with many studies.[32–34] From the analysis of the Ag 3d spectrum in Fig. 2(e), it can be seen that the high-resolution XPS spectrum of Ag 3d was detected in the two strong peaks of the composite catalyst located at around 367.6 eV and 373.8 eV, which are comparable to Ag $3d_{5/2}$ and Ag $3d_{3/2}$, respectively.[35,36] The appearance of these peaks was attributed to the generation of metallic Ag during the modification.

Gannoruwa *et al.*[37] reported that the presence of the Ag surface on TiO_2 was conducive to the photocatalytic oxidation reaction of TiO_2 and the separation of the photo-excited electron–hole pair. Ag produced new electronic states below the TiO_2 conduction band. Surface plasmon resonance (SPR) enhances visible light absorption. It was used as an electron trap to suppress

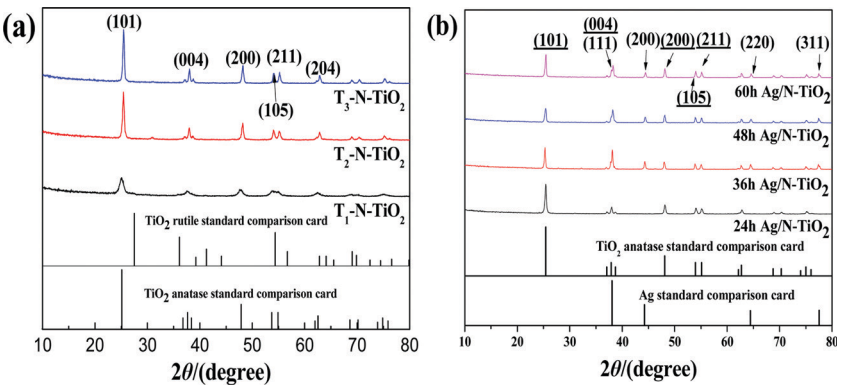

Fig. 1 X-ray diffraction patterns of (a) N-TiO_2 prepared at different reaction temperatures and (b) Ag/N-TiO_2 prepared at different reaction times.

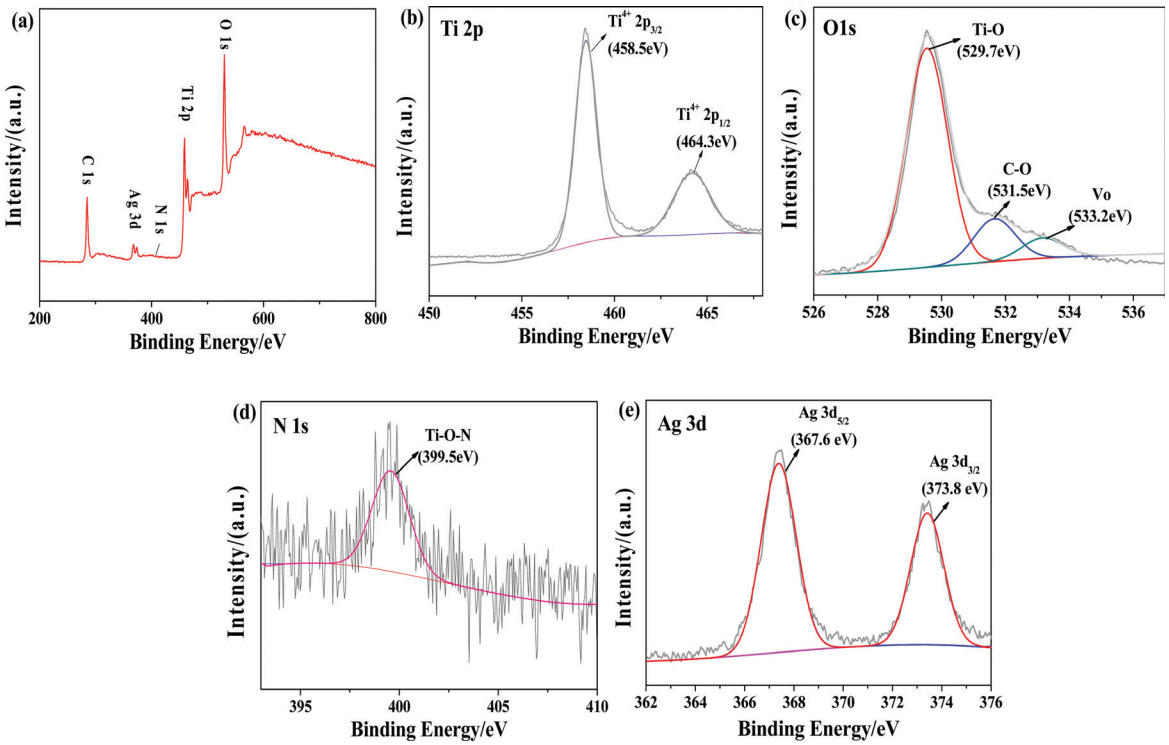

Fig. 2 Ag/N-TiO_2 XPS spectrum (a), Ti 2p (b), O 1s (c), N 1s (d), and Ag 3d (e) XPS spectra.

the electron–hole recombination of the photocatalyst. Ag also provided catalytic sites to promote the reaction of photoelectrons with surface oxygen.

3.1.3. Topography analysis. SEM photographs show that the length of Ag/N-TiO_2 is between 340 and 457 nm, and the diameter of Ag/N-TiO_2 is between 70 and 140 nm, while the diameter calculated using Scherrer's formula is 31.17 nm, obviously deviating from the results observed in SEM photographs. These differences suggest that agglomeration occurs and consequently results in a rod-like shape. Besides, small particles were loaded with explicit Ag crystal lattice[38,39] on the surface. In Fig. 3(c), Ag/N-TiO_2l contains more nanorods. The size of the nanorods is nearly the same as that in Fig. 3(a and b). Fig. 3(d) shows the corresponding HRTEM picture. The lattice fringe with a lattice spacing of 0.33 nm corresponds to the (101) crystal plane of anatase, and the lattice fringe with a lattice spacing of 0.21 nm corresponds to the Ag element (200) crystal plane. The result indicates that the nanomaterial with rod-shaped

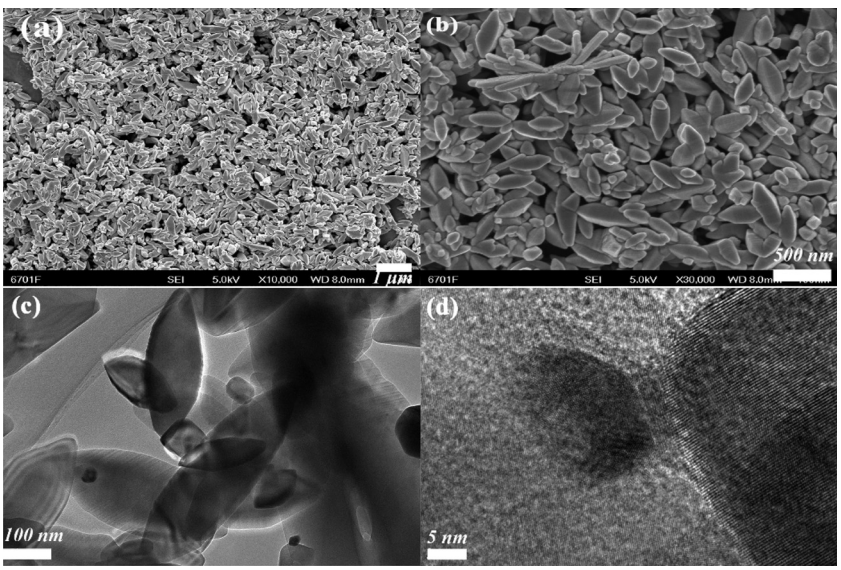

Fig. 3 (a and b) SEM image, (c) TEM image and (d) HRTEM image of Ag/N-TiO_2.

Ag/N-TiO_2 was synthesized. Compared with the undoped TiO_2, the lattice strain of the doped sample has changed, indicating that the introduction of N and Ag causes the distortion of or defects in the TiO_2 crystal.[40,41] The cycled area in Fig. 3(d) presents a lot of fractures on the lattice, implying abundant oxygen vacancies. Milani Moghaddama and Nasirian[42] also reported similar observations. The reason is that when the crystal lattice is affected by the tensile (compressive) force from the surface to the crystal volume, the strain of the crystal lattice is positive or negative, resulting in the change of the crystal grain size and the change of the octahedral block on the TiO_2 lattice. The changes of grain size and lattice strain can also confirm that the *in situ* solvent method was successfully introduced into TiO_2, and the doping of N and Ag in each reaction was the main factor affecting the modification of TiO_2.[43,44] Other studies[45–47] also reported the effect of the crystal structure and grain size of the catalyst on the photocatalytic activity.

3.2. The optical properties and band gap energy

Fig. 4 shows the UV-vis absorption spectra and PL spectra of Ag/N-TiO_2, N-TiO_2, Ag–TiO_2 and pure TiO_2. The intensity of the absorbed radiation reveals the light absorption capacity of the photocatalyst at different wavelengths. Obviously, Ag/N-TiO_2 and Ag–TiO_2 powders are darker in color and exhibit stronger absorption in the wavelength range of 400–600 nm. The reason is the surface plasmon resonance (SPR) effect of silver nanoparticles that appears in the wavelength range of 450–550 nm.[48] As shown in Fig. 5, the calcined N-TiO_2 powder was light yellow and exhibited a low radiation absorption intensity in the visible light region. Yet the white TiO_2 powder displayed no light absorption in this region, indicating that the change of the absorption edge of the TiO_2 semiconductor was related to the type of dopant.

Fig. 4(a) lists the band gap energy in order to compare the band gap energy (E_g) among pristine, Ag-modified and N-doped TiO_2. The calculated E_g value for pristine TiO_2 was 3.2 eV. Once doped by N or Ag, E_g declined to 3.0 eV for N-TiO_2, 2.3 eV for Ag–TiO_2 and 2.1 eV for Ag/N-TiO_2. This result indicated that Ag modification has a more significant effect on reducing the E_g, which corresponded to the red-shift absorption and surface plasmon resonance (SPR) effects. Due to the synergy of N and Ag, the values of E_g of Ag-modified and N-doped samples were the lowest. N doping caused the N 2p band to form a new middle band energy beyond the O 2p valence band coupled with Ag-caused lower E_g, which led to an increase in the visible light response ability.[49]

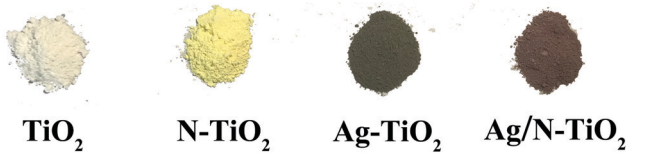

Fig. 5 Color comparison among TiO_2, N-TiO_2, Ag–TiO_2 and Ag/N-TiO_2.

Photoluminescence (PL) spectroscopy is a useful method to study the electronic structure and the electron–hole recombination rate during photocatalysis. Fig. 4(b) shows the PL emission spectra of pure TiO_2, N-TiO_2, Ag–TiO_2, and Ag/N-TiO_2. The obvious absorption wavelengths of the 4 materials were in the range of 480–490 nm. But it is notable that the PL intensity of Ag/N-TiO_2 is much lower than that of pure TiO_2, a proposed explanation for this is that the PL emission intensity of the photocatalyst is directly related to the electron–hole recombination rate, and the introduction of Ag and N efficiently hinders the electron–hole recombination, thus lowering the PL emission intensity of Ag/N-TiO_2. Some studies[43,44,49] also found that this hindrance of the electron–hole recombination could be attributed to Ag modification. In addition, an assumption[50,51] was put forward that Ag acts as an electron captor, possessing a great redox ability to generate various radicals. The overall mechanism is shown in Fig. 6.

What is more, the doping of N and Ag exerts distinct influences on the enhancement of the photocatalytic performance of TiO_2. N doping plays a role in the morphology of the photocatalyst. Ag doping lowers the band gap energy, thereby shifting light absorption to the visible light region and simultaneously hindering the electron–hole recombination. When Ag is modified and N is doped on the TiO_2 crystal lattice, a synergistic effect is produced. Therefore, Ag/N-TiO_2 exhibits a better response to visible light.

3.3. Photocatalytic activity of the catalyst

Fig. 7 shows the relationship between the degradation efficiency of phenol and different doping ratios of Ag/N-TiO_2 (a), *vs.* different

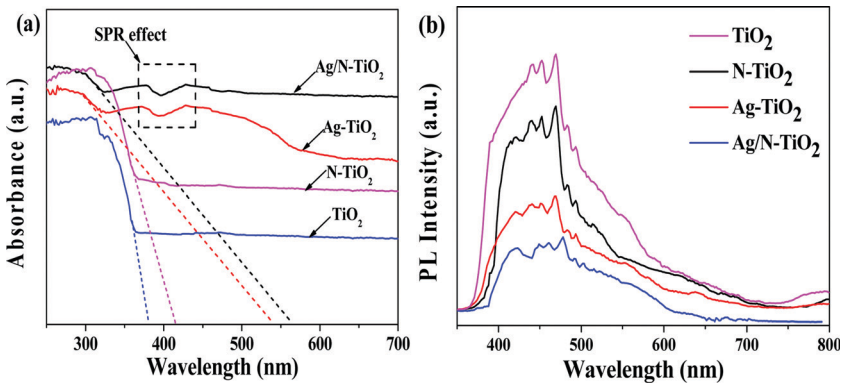

Fig. 4 (a) UV-vis absorption spectra and (b) photoluminescence (PL) emission spectra of TiO_2, N-TiO_2, Ag–TiO_2, and N/Ag–TiO_2.

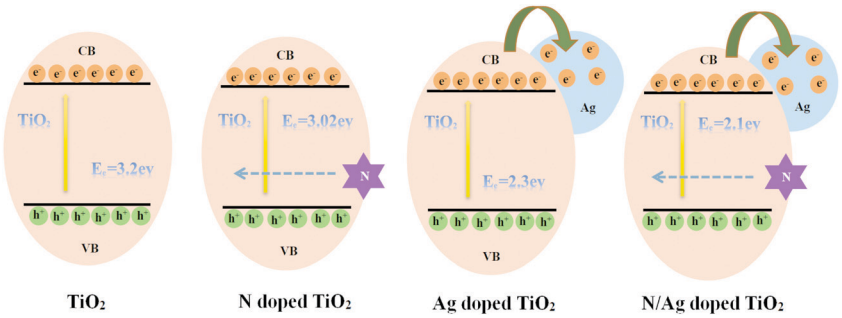

Fig. 6 Schematic diagrams of the band energy structure and the migration of photoexcited electrons in undoped TiO_2, N-TiO_2, Ag–TiO_2, and Ag/N-TiO_2.

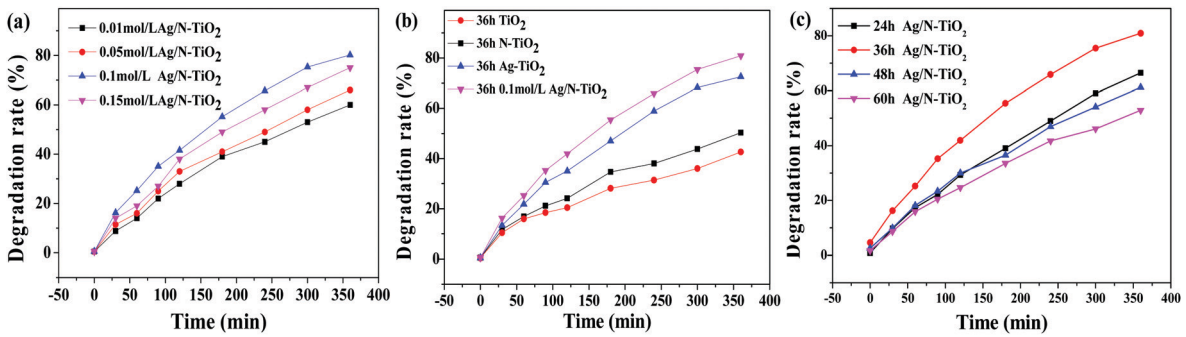

Fig. 7 (a) Under visible light, the degradation effect of Ag/N-TiO_2 with different doping ratios on phenol, (b) the degradation effect of different photocatalysts prepared under hydrothermal reaction for 36 h on phenol, and (c) the phenol removal effect of the Ag/N-TiO_2 material prepared at different hydrothermal reaction times.

doping agents (b) and different reaction times (c). For irradiation, visible light with a wavelength of 420 nm was used. After 6 hours of visible light irradiation, the removal rates of phenol were 60.12%, 66.04% and 74.96% by 0.01 mol L^{-1} $AgNO_3$, 0.05 mol L^{-1} $AgNO_3$ and 0.15 mol L^{-1} $AgNO_3$, respectively. Additionally, Ag/N-TiO_2 doped with 0.1 mol L^{-1} $AgNO_3$ (nTi : nN : nAg = 1 : 0.45 : 0.32) exhibited the best removal efficiency with an 80.21% removal rate against phenol, and the corresponding removal amount was 8.02 mg g^{-1}. In Fig. 7(b), after 6 hours of visible light irradiation, the removal rates of phenol by TiO_2, N-TiO_2, and Ag–TiO_2 were 41.33%, 49.97% and 70.09%, respectively. The results showed that the photocatalytic performance of TiO_2 was enhanced after N or Ag doping, and Ag doping had a greater impact on the photocatalytic performance of TiO_2. The photocatalyst doped with nTi : nN : nAg = 1 : 0.32 : 0.45 displayed the best performance. After obtaining the optimal doping ratio, we continued to find the optimal hydrothermal reaction time. In Fig. 7(c), Ag/N-TiO_2 prepared *via* a hydrothermal reaction for 36 hours exhibited the best phenol removal performance. After 6 hours of visible light irradiation, the phenol removal rate reached 80.21%, while the phenol removal efficiencies of the catalyst subjected to hydrothermal treatment for 24 h, 48 h and 60 h under visible light were 63.78%, 58.97% and 50.06%, respectively.

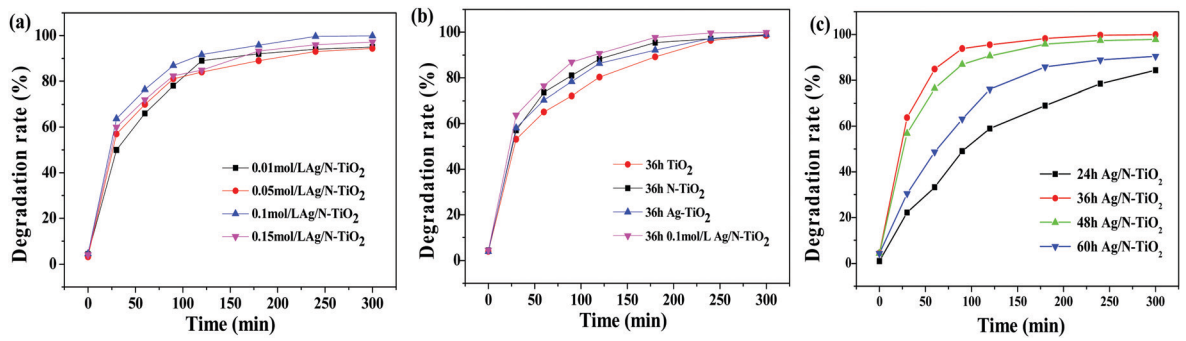

Fig. 8 (a) Under ultraviolet light, the degradation effect of different doping ratios of Ag/N-TiO_2 on phenol, (b) the degradation effect of different photocatalysts on phenol at a hydrothermal reaction time of 36 h, and (c) the phenol removal effect of the prepared Ag/N-TiO_2 material at different hydrothermal reaction times.

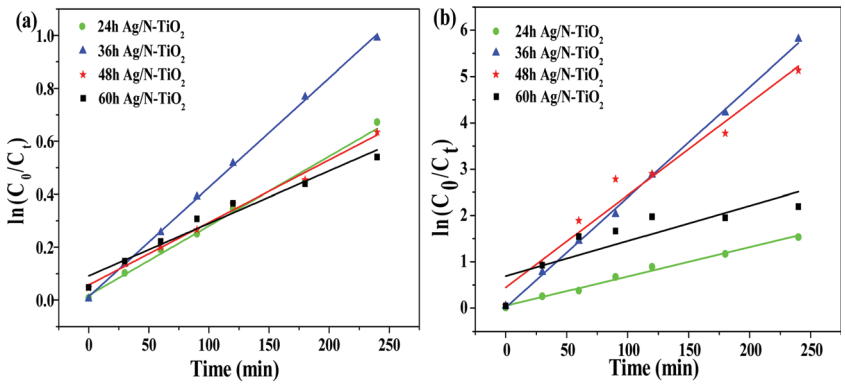

Fig. 9 The Ag/N-TiO_2 nanomaterials prepared at different hydrothermal reaction times are used as the first-order kinetic model for the removal of phenol pollutants under (a) visible light and (b) ultraviolet light.

Fig. 8 shows the relationship of the phenol degradation efficiency with different doping ratios of Ag/N-TiO_2 and reaction times. A 365 nm light source was selected as the ultraviolet light source. In Fig. 8(a), after 90 minutes of ultraviolet light irradiation, the removal rates of phenol were 77.53%, 81.34% and 82.41% by 0.01 mol L^{-1} $AgNO_3$, 0.05 mol L^{-1} $AgNO_3$ and 0.15 mol L^{-1} $AgNO_3$, respectively. Ag/N-TiO_2 doped with 0.1 mol L^{-1} $AgNO_3$ exhibited the best removal efficiency toward phenol, and the phenol removal rate reached 91.5%. In Fig. 8(b), after 90 minutes of ultraviolet light irradiation, the removal rates of phenol by TiO_2, N-TiO_2 and Ag–TiO_2 were 69.89%, 78.96% and 77.68%, respectively. It can be seen from Fig. 8(c) that the Ag/N-TiO_2 prepared *via* a hydrothermal reaction for 36 hours exhibited the best phenol removal effect. A phenol removal rate of 98.85% was achieved after ultraviolet light irradiation for 90 minutes, while the phenol removal efficiency of the catalyst subjected to hydrothermal treatment for 24 h, 48 h and 60 h was 81.98%, 98.86% and 90.06%, respectively, after being irradiated with ultraviolet light for 5 h.

3.4. Kinetic study of the photocatalytic reaction

In this study the first-order kinetic equation was used to fit the photocatalytic performance of several materials.[52] The results are shown in Fig. 9. The Ag/N-TiO_2 material with Ag modification had a significantly higher degradation rate against phenol than pristine TiO_2 did, consistent with the discussions in section 3.3. Hence, the formation of a heterojunction between Ag/N-TiO_2 and the surface plasmon resonance effect of Ag nanoparticles broadened the visible light response range, and the band gap difference promoted photo-generated charge migration and improved the photocatalytic efficiency. With R^2 being the related linear fitting coefficient and k being the first-order reaction rate constant of the photocatalytic degradation reaction, which reflects the degree of degradation, the reaction rate is proportional to the first power of the reactant concentration:[53] $dC/dt = k_C$, that is, $\ln(C_0/C_t) = k_t$, where C_0 and C_t are the phenol concentrations at the initial time and objective time, respectively. Tables 1 and 2 present the detailed data of kinetics.

3.5. Factors affecting the photocatalysis of Ag/N-TiO_2

Active free radicals are important oxidants produced by irradiation upon photocatalysis. Current opinions consider them as the main reagents to degrade contaminants. In order to detect the key photocatalytic mineralization of phenol, three main strong oxidants, namely, superoxide radicals ($^{\bullet}O_2^-$), hydroxyl radicals ($^{\bullet}OH$), and holes (h^+), produced during the reaction were studied in detail.[54] The reaction inhibitors, 100 mg L^{-1} benzoquinone, 150 mg L^{-1} isopropanol, and 150 mg L^{-1} EDTA-Na_2, were selected as the radical

Table 1 Photocatalytic first-order kinetic parameters of phenol at different temperatures under visible light conditions

Material	First order dynamic model	K/min	R^2
24 h Ag/N-TiO_2	$\ln(C_0/C_t) = 2.63 \times 10^{-3}t + 1.78 \times 10^{-2}$	2.63×10^{-3}	0.9871
36 h Ag/N-TiO_2	$\ln(C_0/C_t) = 4.13 \times 10^{-3}t - 1.27 \times 10^{-2}$	4.13×10^{-3}	0.9991
48 h Ag/N-TiO_2	$\ln(C_0/C_t) = 2.36 \times 10^{-3}t + 5.71 \times {}^{1}10^{-2}$	2.36×10^{-3}	0.9819
60 h Ag/N-TiO_2	$\ln(C_0/C_t) = 1.98 \times 10^{-3}t - 9.15 \times 10^{-2}$	1.98×10^{-3}	0.9612

Table 2 Photocatalytic first-order kinetic parameters of phenol at different temperatures under ultraviolet light

Material	First order dynamic model	K/min	R^2
24 h Ag/N-TiO_2	$\ln(C_0/C_t) = 6.34 \times 10^{-3}t - 4.89 \times 10^{-3}$	6.34×10^{-3}	0.9891
36 h Ag/N-TiO_2	$\ln(C_0/C_t) = 2.38 \times 10^{-2}t - 8.59 \times 10^{-3}$	2.38×10^{-2}	0.9993
48 h Ag/N-TiO_2	$\ln(C_0/C_t) = 1.99 \times 10^{-2}t + 4.46 \times 10^{-1}$	1.99×10^{-2}	0.9825
60 h Ag/N-TiO_2	$\ln(C_0/C_t) = 7.59 \times 10^{-3}t + 6.91 \times 10^{-1}$	7.59×10^{-3}	0.8539

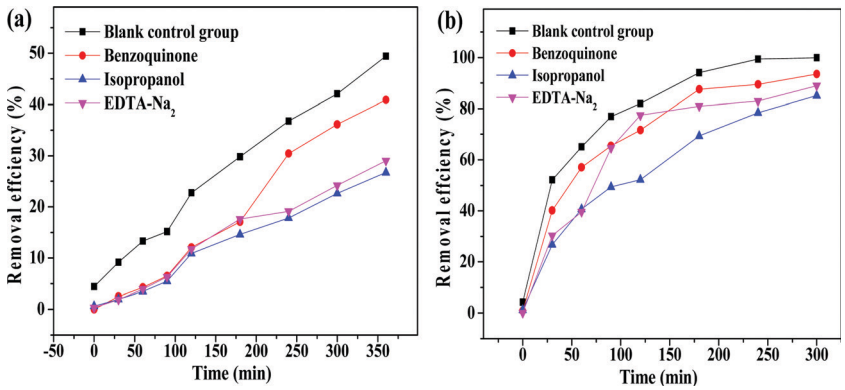

Fig. 10 Study on the mechanism of photocatalytic oxidation of phenol by Ag/N-TiO_2 under (a) visible light irradiation and (b) ultraviolet light irradiation.

captors, and a preliminary test proved these concentrations as efficient for radical capture.[54] Meanwhile, a blank group was also set for comparison. The LED light source (with a wavelength of 420 nm and an incident intensity of 8.3 μW cm^{-2} as the visible light source, and with a wavelength of 365 nm and an incident intensity of 7.4 μW cm^{-2} as the ultraviolet light source) was used for irradiation (for 6 h). In Fig. 10, the addition of the isopropanol inhibitor had the strongest inhibitory effect on the reaction under either ultraviolet light irradiation or visible light irradiation, meaning that the hydroxyl radical (•OH) was the main factor in phenol mineralization. Also, noticeably, some studies[50,55] found that Ag addition significantly enhanced •OH generation, which may be one reason for the better performance of Ag/N-TiO_2.

3.6. Mineralization performance

Mineralization toward contaminants is a critical factor in determining the performance of a photocatalyst. In addition, it is usually evaluated in terms of residual total organic carbon concentration (TOC).[56–58] Fig. 11 depicts the mineralization performance against phenol by TiO_2, N-TiO_2, Ag–TiO_2 and Ag/N-TiO_2 under 6 hours of visible/ultraviolet light irradiation.

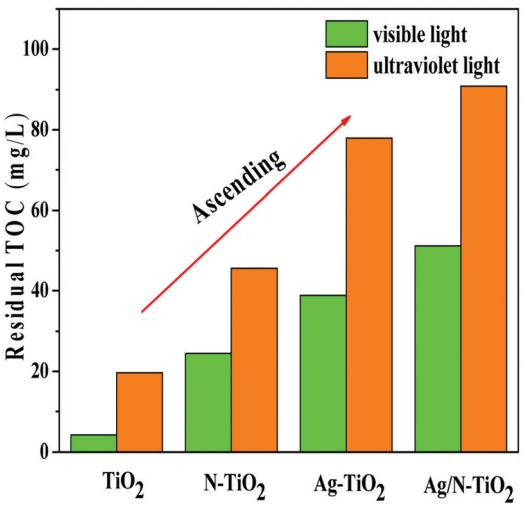

Fig. 11 The mineralization properties of TiO_2, N-TiO_2, Ag–TiO_2, and Ag/N-TiO_2 toward phenol.

Under visible light irradiation, the mineralization rates toward phenol were 4.20%, 24.50%, 38.85% and 51.20% by TiO_2, N-TiO_2, Ag–TiO_2 and Ag/N-TiO_2, while they were 19.62%, 45.65%, 78.92% and 90.86%, respectively, under ultraviolet light. Among the 4 materials, Ag/N-TiO_2 exhibited the best phenol mineralization under either visible or ultraviolet light. Considering the phenol removal efficiency, Ag/N-TiO_2 removed nearly 100% phenol while mineralizing 90.86% phenol under complex light source illumination, denoting the potent photocatalytic performance of Ag/N-TiO_2. However, the inferior mineralization efficiency obtained under visible light compared with that achieved under ultraviolet light (51.20% *vs.* 90.86) implied more active free radicals produced under ultraviolet light irradiation. This observation agreed with commonly reported results.[57,59]

Phenol is a contaminant that is commonly being studied, and its concrete degradation products are also being investigated widely. Recently, 4 intermediates—catechol, resorcinol, hydroquinone, and benzoquinone—have been commonly proposed.[57–60] In this regard, we detected the existence of the 4 intermediates by HPLC and analyzed the concentrations of these intermediates with irradiation time, as shown in Fig. 12. Under visible light irradiation, hydroquinone, catechol and resorcinol were the main degradation intermediates. Their concentrations increased with irradiation at the early photocatalysis stage, gradually reaching the peak after 240 minutes of irradiation, and then decreased. Catechol and hydroquinone were the final products after 300 minutes of irradiation, whereas benzoquinone molecules were nearly eliminated. In contrast, phenol quickly degraded into various intermediates under ultraviolet light. The intermediates were hydroquinone, catechol, and benzoquinone, similar to those observed under visible light irradiation. In addition, the concentrations of these intermediates were much lower than those of their counterparts under visible light irradiation, implying that phenol was degraded into nontoxic small molecules easily under ultraviolet light. The results were in accordance with the analysis of the mineralization properties. Based on the analysis of the results obtained for intermediates, we proposed a potential degradation pathway for phenol in our study as shown in Fig. 13 (mobile phase: acetonitrile : water = 1 : 9, our test demonstrated that the flow rate of 0.8 mL min^{-1} efficiently separated the aforementioned 4 intermediates, and the absorption wavenumber was set at

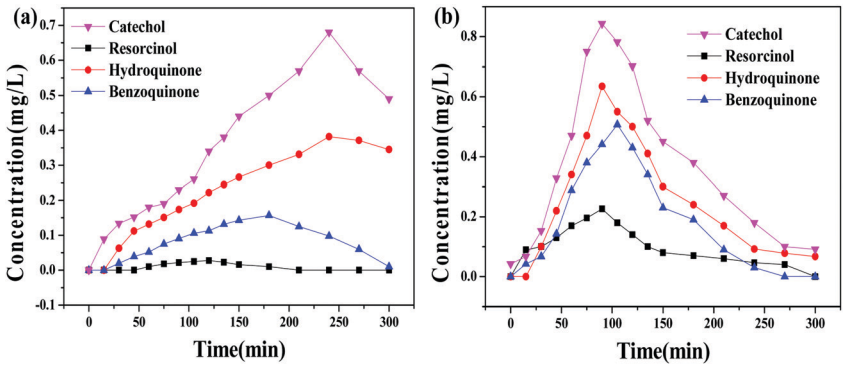

Fig. 12 Concentration changes of intermediate products in the process of Ag/N-TiO_2 photocatalytic degradation of phenol under (a) visible light irradiation and (b) ultraviolet light irradiation.

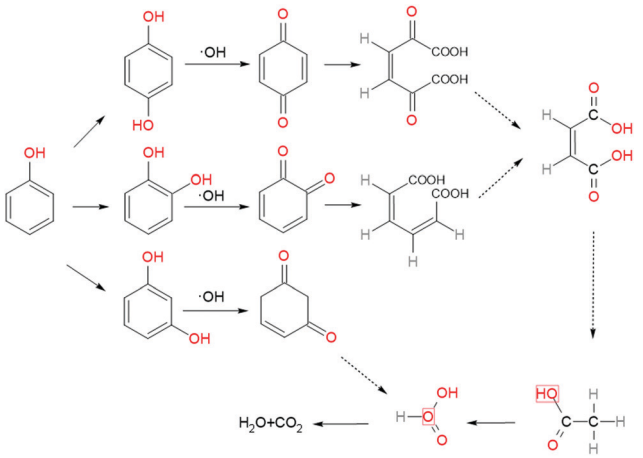

Fig. 13 Proposed degradation pathway for phenol.

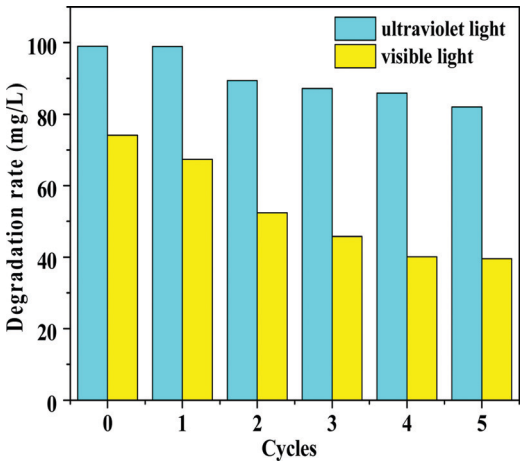

Fig. 14 Reusability of Ag/N-TiO_2.

280 nm; the retention times of hydroquinone, catechol, resorcinol, and benzoquinone were 3.116 min, 3.69 min, 4.5 min and 6.378 min, respectively).

3.7. Recycling performance

Regeneration performance is an important indicator for evaluating the economic operability of a catalyst.[60] In this study, Ag/N-TiO_2 was recycled 5 times. The used Ag/N-TiO_2 was rinsed with deionized water and ethanol several times, and then vacuum-dried at 60 °C. The recycling results are shown in Fig. 14. In the process of UV degradation, the degradation in the first cycle was almost complete, and in the subsequent cycles it slowly declined down to 89.84%, 84.12%, 83.33%, and 82.89%, respectively. In the process

Table 3 Comparison of the phenol removal ability of various TiO_2 photocatalysts

Photocatalyst	Pollutant	Light type	Degradation time for pollutants (min)	Degradation rate for pollutants (%)	Mineralization capacity (%)	Ref.
H_2O_2/TNSs/TiO_2	Phenol	UV-A lamp	—	—	—	61
		Visible light	350	97.12		
TiO_2/AC	Phenol	UV light	120	89.7	—	62
		Visible light	—	—	—	
4% PF/TiO_2	Phenol	UV lamp	180	88.00	—	63
		Natural sunlight	450	62.80		
Ag_3PO_4/TiO_2-OV	Phenol	UV lamp	—	—	—	64
		Visible light	90	61.00	68.00	
[FeII(dpbpy)$(phen)_2$]/TiO_2	Phenol	UV lamp	—	—	—	65
		Visible light	180	97.00	71.00	
TiO_2/H_2O_2	Phenol	UV lamp	—	—	—	66
		Visible light	350	97.12	—	
Ag/N-TiO_2	Phenol	UV light	300	99.02	90.86	This work
		Visible light	350	80.21	51.20	

of visible light degradation, the degradation in the first cycle was 75.84%, and in the subsequent cycles it slowly decreased to 57.01%, 49.26%, 43.74%, and 42.69%, respectively. After 5 cycles, a certain degradability remained, so Ag/N-TiO_2 has a repeatable operability.

The photocatalytic performance of Ag/N-TiO_2 in the removal of phenol reported in other studies is summarized in Table 3. From Table 3, it can be seen that Ag/N-TiO_2 exhibits good performance in phenol degradation under either ultraviolet light or visible light irradiation, despite the highest performance. At present, there are only a few reports on the effect of metal/non-metal co-doped TiO_2 as a photocatalyst on the removal of phenol under ultraviolet/visible conditions.

4. Conclusion

In this study, we prepared a silver-modified and N-doped TiO_2 material with oxygen vacancies by a modified-hydrothermal method. The batch experimental results showed that the optimal synthesis temperature is 210 °C and the optimal ratio of the feedstock addition is $n(\mathrm{Ti}):n(\mathrm{N}):n(\mathrm{Ag}) = 1:0.45:0.32$. Phenol degradation by this Ag/N co-doped TiO_2 was enhanced compared with pristine TiO_2, and several conclusions were drawn from the analysis of the results from characterizations and well-designed experiments, which are as follows:

(1) The characterization results presented shuttle-like TiO_2 nanorods with multiple oxygen vacancies. The Ti element exists as Ti^{4+} in the crystal lattice, in which N is successfully embedded and Ag particles are well dispersed on the nanorod surface.

(2) The introduction of Ag and N narrowed the band gap of TiO_2 from 3.2 eV to 2.1 eV and strengthened its response to visible light. Meanwhile, the photo-generated electron–hole recombination was efficiently impeded.

(3) The degradation efficiency and mineralization efficiency against phenol by the optimal material reached 80.2% and 38.86% under visible light, while under ultraviolet light the degradation efficiency and mineralization efficiency against phenol were nearly 100% and 90.86%, respectively. The recycling tests also proved it to be an economical catalyst.

(4) The photo-generated electrons were captured by Ag particles, thus triggering a chain reaction generating superoxide radicals ($^{\bullet}O_2^-$), hydroxyl radicals ($^{\bullet}OH$), and holes (h^+). In addition, $^{\bullet}OH$ was attested as the main factor in phenol degradation.

Conflicts of interest

The authors declare that they have no competing interests.

Acknowledgements

The authors are grateful for the financial aid from the Innovation and Entrepreneurship Talent Project of Lanzhou (2019-RC-21), the Longyuan Youth Innovation and Entrepreneurship Talent Project (2020RCXM180) and the Key Research and Development Project of Gansu Province (17YF1GA014).

Notes and references

1 W. G. Tu, W. L. Guo, J. Q. Hu, H. C. He, H. J. Li, Z. S. Li, W. j. Luo, Y. Zhou and Z. G. Zou, *Mater. Today*, 2020, **33**, 75–86.
2 M. Ghosh, M. Lohrasbi, S. S. C. Chuang and S. C. Jana, *ChemCatChem*, 2016, **8**, 2525–2535.
3 Y. Jiang, Y. C. Zhou and H. B. Xue, *Environ. Eng.*, 2019, **37**, 114–118.
4 S. Tanigawa and H. Irie, *Appl. Catal., B*, 2016, **180**, 1–5.
5 A. Y. Zhang, Y. Zhou, X. Liu, N. H. Huang and H. H. Niu, *J. Hazard. Mater.*, 2020, **390**, 122159.
6 C. Tao, Q. p. Jia, B. Han and Z. l. Ma, *Chem. Eng. Sci.*, 2020, **214**, 115348.
7 N. Sharotri, D. Sharma and D. Sud, *J. Mater. Res. Technol.*, 2019, **8**, 3995–4009.
8 L. C. Sim, K. H. Leong, P. Saravanan and S. Ibrahim, *Appl. Surf. Sci.*, 2015, **358**, 122–129.
9 Y. Li, W. Zhang and J. F. Niu, *ACS Nano*, 2012, **6**, 5164–5173.
10 V. Etacheri, G. Michlits, M. K. Seery, S. J. Hinder and S. C. Pillai, *ACS Appl. Mater. Interfaces*, 2013, **5**, 1663–1672.
11 N. S. Peighambardoust, S. K. Asl, R. Mohammadpour and S. K. Asl, *Electrochim. Acta*, 2018, **270**, 245–255.
12 G. Nagaraj, A. Dhayal Raj, A. Albert Irudayaraj and R. L. Josephine, *Optik*, 2019, **179**, 889–894.
13 A. A. Ashkarran, M. Kavianipour and S. M. Aghigh, *J. Cluster Sci.*, 2010, **21**, 753–766.
14 S. Bouhadoun, C. Guillard, F. Dapozze, S. Singh, D. Amans, J. Bouclé and N. Herlin-Boime, *Appl. Catal., B*, 2015, **175**, 367–375.
15 M. Z. Ge, C. Y. Cao, S. H. Li, Y. X. Tang, L. N. Wang, N. Qi, J. Y. Huang, K. Q. Zhang, S. S. Al Deyabe and Y. K. Lai, *Nanoscale*, 2016, **8**, 5226–5234.
16 P. Wang, B. Huang, Y. Dai, J. Wei and M. H. Whangbo, *Phys. Chem. Chem. Phys.*, 2012, **14**, 9813–9825.
17 Y. Wang, M. M. Zhang, S. H. Lv, X. Q. Li, D. B. Wang and C. X. Song, *ACS Omega*, 2020, **5**(23), 13994–14005.
18 S. Sakthivel, M. V. Shankar, M. Palanichamy, B. Arabindoo, D. W. Bahnemann and V. Murugesan, *Water Res.*, 2004, **38**, 3001–3008.
19 L. F. Wei, C. L. Yu, Q. H. Zhang, H. Liu and Y. Wang, *J. Mater. Chem. A*, 2018, **6**, 22411–22436.
20 J. J. Li, B. Weng, S. C. Cai, J. Chen, H. P. Jia and Y. J. Xu, *J. Hazard. Mater.*, 2018, **342**, 661–669.
21 H. Xu, M. M. Ding, W. Chen, Y. Li and K. Wang, *Sep. Purif. Technol.*, 2018, **195**, 70–82.
22 N. S. Peighambardoust, S. K. Asl, R. Mohammadpour and S. K. Asl, *Electrochim. Acta*, 2018, **270**, 245–255.
23 M. Sharma and Nihal, *Mater. Today: Proc.*, 2020, **3**, 3390–3396.
24 J. Senthilnathan and L. Philip, *Chem. Eng. J.*, 2010, **161**, 83–92.
25 O. Ibukun and H. K. Jeong, *Chem. Phys. Lett.*, 2020, **744**, 137234.
26 H. U. Lee, S. C. Lee, S. Choi, B. Son, S. M. Lee, H. J. Kim and J. Lee, *Chem. Eng. J.*, 2013, **228**, 756–764.
27 E. Fernandes, S. Contreras, F. Medina, R. C. Martins and J. Gomes, *Process Saf. Environ. Prot.*, 2020, **138**, 80–89.

28 K. J. Shao, Y. J. Wang, M. Iqbal, L. Lin, K. Wang, X. H. Zhang, M. He and T. He, *Appl. Surf. Sci.*, 2018, **434**, 717–724.
29 X. F. Lei, X. X. Xue and H. Yang, *Appl. Surf. Sci.*, 2014, **321**, 396–403.
30 M. Ghosh, J. W. Liu, S. S. C. Chuang and S. C. Jana, *ChemCatChem*, 2018, **10**, 3305–3318.
31 L. Y. Shen, *Preparation and application of a black TiO_2/g-C_3N_4 catalyst,* Heilongjiang University, Heilongjiang, 2017, pp. 28–31.
32 T. Xu, M. Wang and T. Wang, *J. Wuhan Univ. Technol., Mater. Sci. Ed.*, 2019, **34**, 55–63.
33 S. M. Reda, M. Khairy and M. A. Mousa, *Arabian J. Chem.*, 2020, **13**, 86–95.
34 H. Wang and Y. Hu, *Int. J. Photoenergy*, 2013, 1–6.
35 X. Y. Zhang, M. Li, X. J. He, X. B. Huang, R. Q. Hang and B. Tang, *Mater. Des.*, 2014, **65**, 600–605.
36 A. Zielinska, E. Kowalska, J. Sobczak, I. Łącka, M. Gazda, B. Ohtani, J. Hupka and A. Zaleska, *Sep. Purif. Technol.*, 2010, **45**, 155–162.
37 A. Gannoruwa, B. Ariyasinghe and J. Bandara, *Catal. Sci. Technol.*, 2016, **6**, 479–487.
38 H. Y. Si, *Preparation of nano-composite by using surface functionalization to modify nano-particles*, Lanzhou University, Lanzhou, 2009.
39 M. M. Momeni, Y. Ghayeb and S. Gheibee, *Ceram. Int.*, 2017, **43**, 564–570.
40 X. D. Wang, K. Zhang, X. L. Guo, G. D. Shen and J. Y. Xiang, *New J. Chem.*, 2014, **38**, 6139–6146.
41 X. W. Cheng, X. J. Yu, Z. P. Xing and J. F. Wan, *Energy Procedia*, 2012, **16**, 598–605.
42 H. M. Moghaddam and S. Nasirian, *Nanosci. Methods*, 2012, **1**, 201–212.
43 X. H. Gao, B. H. Zhou and R. F. Yuan, *Environ. Eng. Res.*, 2015, **20**, 329–335.
44 S. I. Mogal, V. G. Gandhi, M. K. Mishra, S. Tripathi, T. Shripathi, P. A. Joshi and D. O. Shah, *Ind. Eng. Chem. Res.*, 2014, **53**, 5749–5758.
45 G. L. Li, J. Li, G. Li and G. B. Jiang, *J. Mater. Chem. A*, 2015, **3**, 22073–22080.
46 X. W. Cheng, X. J. Yu, Z. P. Xing and L. S. Yang, *Arabian J. Chem.*, 2016, **9**, S1706–S1711.
47 T. Y. Lee, C. Y. Lee and H. T. Chiu, *ACS Omega*, 2018, **3**, 10225–10232.
48 Y. Wang, C. X. Feng, M. Zhang, J. J. Yang and Z. J. Zhang, *Appl. Catal., B*, 2010, **100**, 84–90.
49 J. H. Hu, C. Y. Ma and J. L. Wang, *J. Compos.*, 2020, 37.
50 D. Li, X. Y. Zhang and W. Zhang, *Chem. Eng. J.*, 2020, **405**, 126867.
51 D. Komaraiah, E. Radha, J. Sivakumar, M. V. Ramana Reddy and R. Sayanna, *Opt. Mater.*, 2020, **108**, 110401.
52 M. M. Zou, H. H. Liu, L. Feng, F. Q. Xiong, T. J. Thomas and M. H. Yang, *Microporous Mesoporous Mater.*, 2017, **240**, 137–144.
53 J. Carbajo, A. Bahamonde and M. Faraldos, *Mol. Catal.*, 2017, **434**, 167–174.
54 S. Garga, M. Yadav, A. Chandra, S. Gahlawat, P. P. Ingoled, Z. Pap and K. Hernadi, *Ecotoxicol. Environ. Saf.*, 2018, **165**, 357–366.
55 Y. Sun, Y. Gao, J. Y. Zeng, J. Guo and H. Wang, *Mater. Lett.*, 2020, **279**, 128506.
56 D. L. Jiang, J. J. Zhu and M. Chen, *J. Colloid Interface Sci.*, 2014, **417**, 115–120.
57 K. Priyanka, N. Remya and M. Behera, *J. Cleaner Prod.*, 2019, **235**, 1–10.
58 G. J. Rincón and E. J. L. Motta, *Heliyon*, 2019, **5**, e01966.
59 G. L. Li, J. Li, G. Li and G. B. Jiang, *J. Mater. Chem. A*, 2015, **3**, 22073–22080.
60 M. Xu, L. Han and S. J. Dong, *ACS Appl. Mater. Interfaces*, 2013, **5**, 12533–12540.
61 M. Zulfiqar, S. Sufian, N. E. Rabat and N. Mansor, *J. Mol. Liq.*, 2020, **308**, 112941.
62 K. Naeem and F. Ouyang, *J. Environ. Sci.*, 2013, **25**, 399–404.
63 H. J. Li, J. M. Ji, C. Cheng and K. Liang, *J. Phys. Chem. Solids*, 2018, **122**, 25–30.
64 Y. Z. Li, P. F. Wang, C. P. Huang, W. F. Yao, Q. Wu and Q. J. Xu, *Appl. Catal., B*, 2017, **205**, 489–497.
65 X. Y. Wang, Y. N. Sun, L. Yang, Q. K. Shang, D. Wang, T. T. Guo and Y. H. Guo, *Sci. Total Environ*, 2019, **656**, 1010–1020.
66 N. Areerachakul, S. Sakulkhaemaruethai, M. A. H. Johir, J. Kandasamy and S. Vigneswaran, *J. Water Process. Eng.*, 2019, **27**, 177–184.

